Impact of interfaces on magnetic properties of Gdx(Fe90Co10)1–x alloys

Jean-Loïs Bello, Daniel Lacour, Sylvie Migot, Jaafar Ghanbaja, Stéphane Mangin, Michel Hehn

Applied Physics Letters

RESEARCH ARTICLE | NOVEMBER 21 2022

Impact of interfaces on magnetic properties of $Gd_x(Fe_{90}Co_{10})_{1-x}$ alloys

Jean-Loïs Bello ; Daniel Lacour ; Sylvie Migot; Jaafar Ghanbaja; Stéphane Mangin ; Michel Hehn

Appl. Phys. Lett. 121, 212402 (2022)
https://doi.org/10.1063/5.0125011

AIP Publishing

Applied Physics Letters ARTICLE scitation.org/journal/apl

Impact of interfaces on magnetic properties of $Gd_x(Fe_{90}Co_{10})_{1-x}$ alloys

Cite as: Appl. Phys. Lett. **121**, 212402 (2022); doi: 10.1063/5.0125011
Submitted: 9 September 2022 · Accepted: 7 November 2022 ·
Published Online: 21 November 2022

Jean-Loïs Bello, Daniel Lacour, Sylvie Migot, Jaafar Ghanbaja, Stéphane Mangin, and Michel Hehn[a)]

AFFILIATIONS

Université de Lorraine, CNRS, IJL, F-54000 Nancy, France

[a)]Author to whom correspondence should be addressed: michel.hehn@univ-lorraine.fr

ABSTRACT

A 5 nm thick ferrimagnetic film made of amorphous rare-earth transition-metal alloys $Gd_x(Fe_{90}Co_{10})_{1-x}$ was grown by physical vapor deposition. Its magnetic properties (coercivity, perpendicular magnetic anisotropy, and compensation composition at room temperature) were investigated for various buffer and capping layers in contact with a ferrimagnetic thin film. While $Gd_x(Fe_{90}Co_{10})_{1-x}$ appears to be amorphous for all the samples, it appears that (111) textured Cu is the best material to promote perpendicular magnetization. The large compensation composition change as a function of the magnetic film interface at room temperature is analyzed in terms of polarizability of the surrounding buffer and capping materials.

Amorphous rare-earth transition-metal (RE-TM) alloys are a very interesting class of materials since their magnetic properties can be finely tuned by their chemical composition and temperature.[1,2] They show large magneto-optical and spintronic effects and are useful to realize devices to propagate magnetic textures or build THz oscillators.[3] One material of particular interest is the GdFeCo ferrimagnetic alloy. In this material, the magnetic moment of the rare-earth sublattice (Gd) is antiferromagnetically exchange coupled to one of the transition-metals (FeCo).[5] The resulting net magnetization and coercivity can easily be tuned by changing the temperature or the RE concentration.[6] Magnetization compensation, i.e., zero net magnetization, can be achieved for specific composition or temperature.

Recently, this material has attracted much interest thanks to its light and current induced switching properties.[4,7,8] While the bulk properties have been largely reported in the literature,[6] its recent use as ultrathin films led to a variability of properties: variability of composition for room temperature compensation or in-plane/out-of-plane magnetization stabilization for a given chemical composition. In this paper, we study those properties, keeping the thickness of GdFeCo fixed to 5 nm and changing both the concentration of Gd and the materials in contact with GdFeCo. We show that the variability of properties can be related to the buffer and capping layers used in the multilayer while GdFeCo keeps its amorphous state.

SiO_2//Ta(5 nm)/Y(ynm)/$Gd_x(Fe_{90}Co_{10})_{1-x}$(5 nm)/Z(znm)/Pt(5 nm) heterostructures were grown by magnetron sputtering. Before the multilayer is deposited, the surface of the substrate surface is etched by a RF Ar plasma at a pressure of 10^{-2} mbar for 5 min. During deposition, the sample holder is rotated at several tens of revolutions per minute to ensure uniform layer thickness. The 5 nm thick $Gd_x(Fe_{90}Co_{10})_{1-x}$ layer was co-sputtered from highly pure Gd, Fe, and Co targets. The composition was controlled by adjusting the power of each target and was calibrated before deposition. The atomic composition was varied systematically in a range of $22\% < x < 33\%$. In all multilayers, a buffer of tantalum (Ta) is sputtered before the magnetic layer promotes layer adhesion, block diffusion of Si and O_2 from the substrate, and erase any texture that could come from the substrate. Also, a platinum (Pt) film is added over as a capping layer to prevent against oxidation. Y and Z have been varied by choosing Cu (copper), Pt, Ta, or Ir (iridium). For each sample, we measured the magnetic hysteresis loop at room temperature with a Kerr laser setup in the polar geometry. The effective magnetic anisotropy will result from the competition between the magnetic anisotropies and the shape anisotropy related to the demagnetization field of the thin film. From the shape of the loop, the direction of the effective magnetic anisotropy is extracted: out of the plane (OOP) if the loop is square with hysteresis and in the plane (IP) if the loop is linear. From the loops, we also determine the coercive fields as well as the saturation fields. The former is expected to diverge at the magnetization compensation. Since our Kerr setup mainly probes the TM sub-lattice, it is also straightforward to deduce which sub-lattice dominates the magnetization of the sample as a function of x. Finally, due to the low saturation magnetization and reduced thickness of the $Gd_x(Fe_{90}Co_{10})_{1-x}$ alloy thin film, the magnetic moment

and so the magnetic anisotropies could not be quantified, and the magnetic signal of the substrate is too large.

Figure 1(a) reports the evolution of the coercive field of SiO_2//Ta(5 nm)/Y(5 nm)/$Gd_x(Fe_{90}Co_{10})_{1-x}$(5 nm)/Z(5 nm)/Pt(5 nm) multilayers with various Y and Z interfaces. Only samples that exhibit effective perpendicular magnetic anisotropy (PMA) are reported, and samples with in-plane magnetization in the range $22\% < x < 33\%$ are not shown in the graph. The vertical lines represent the change between CoFe-rich samples and Gd-rich composition, respectively, on the left and right sides of the lines, for each couple of interfaces. The analysis of the Kerr hysteresis loops provides the compositional ranges in which the alloy is TM or RE dominant. A visual representation of TM or RE dominance is reported in Fig. 1(b). An obvious and clear correlation with the coercive field is observed.

Starting with SiO_2//Ta(5 nm)/$Gd_x(Fe_{90}Co_{10})_{1-x}$(5 nm)/Pt(5 nm), no PMA could be demonstrated for $x < 24.4\%$ or $x > 29.2\%$ since only hysteresis loops' characteristics of in plane effective magnetic anisotropy could be observed (Fig. 2). For $24.4\% < x < 29.2\%$, a curvy loops characteristic of multi-domains' states with PMA is observed. At $x = 29.2\%$, the sign of the loop changes indicates that the composition of magnetic compensation has been passed. A possible explanation of those magnetic response is the low anisotropy of the magnetic layer and the presence of DMI (Dzyaloshinskii–Moriya Interaction) at the $Gd_x(Fe_{90}Co_{10})_{1-x}$/Pt interface. Inserting Ta at this interface changes drastically the magnetic response. First, square hysteresis loops with the field applied along the direction perpendicular to the film could be observed for two compositions on both sides of the compensation. Second, the composition for compensation moved from 29.2% to 24% (Fig. 1).

Adding Cu at the $Gd_x(Fe_{90}Co_{10})_{1-x}$ interfaces has a major impact on the magnetic properties. Comparing to two Ta interfaces, inserting Cu either at the lower interface [Fig. 1(a), orange circle], at the upper interface [Fig. 1(a), blue circle], or at both interfaces [Fig. 1(a), red circle] improves the PMA. In the latter case, PMA is maintained for a very wide range of composition from $x = 20.2\%$ to $x = 30.4\%$. Removing one interface leads to a reduction in the window of x for which PMA exists. As a result, Cu appears to be the best candidate to promote PMA. By adding one or two Cu interfaces, we can clearly observe that the concentration for magnetic compensation shifts to a higher concentration of Gd.

For all other samples studied in this paper, a Cu interface is retained to promote PMA. The other interface was modified to check

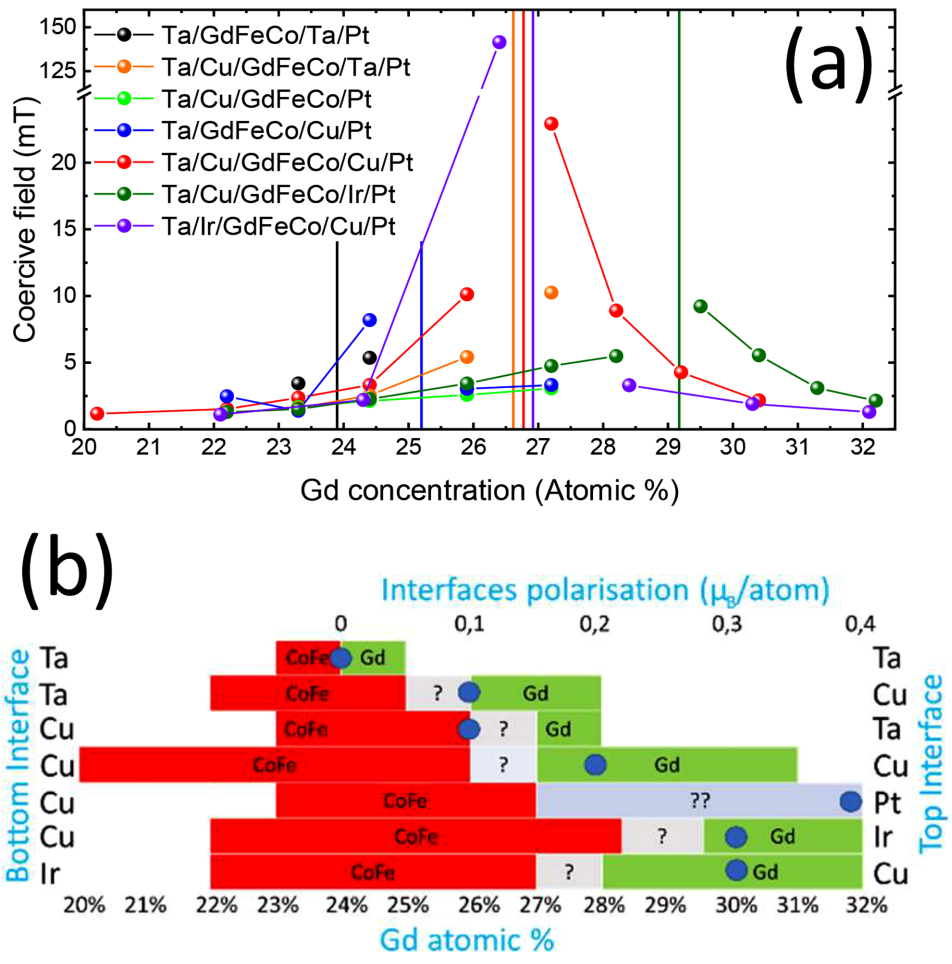

FIG. 1. (a) Coercive field as a function of the Gd concentration for 5 nm thick GdFeCo layers with different interfaces. (b) Summary of the magnetic behavior as a function of the bottom interface material (left column) and top interface material (right column): red—CoFe dominant, green—Gd dominant, white in plane. The blue points are the calculated interface magnetic polarizations considering both interfaces.

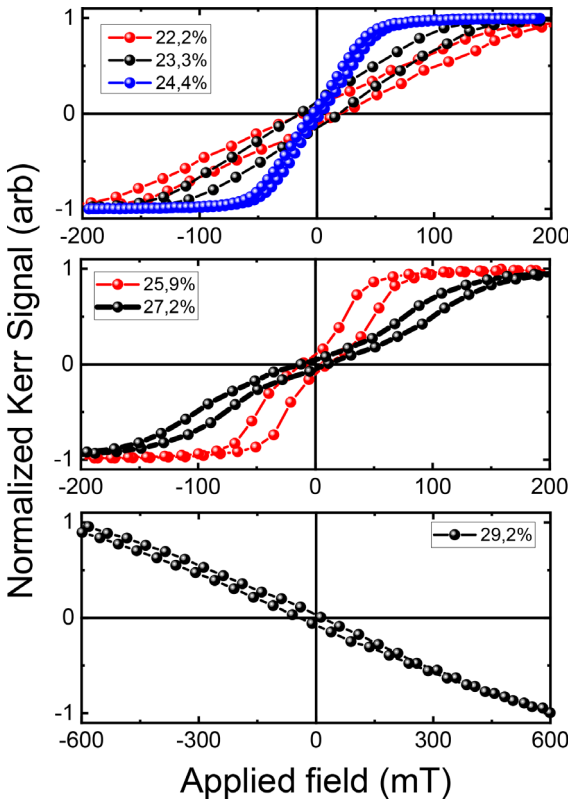

FIG. 2. Hysteresis loops for Ta/GdFeCo/Pt samples at different compositions measured by Kerr magnetometry.

its impact on the magnetic properties. Thus, we tested the insertion of Pt or Ir. For example, the use of Cu is mandatory for the Ta/GdFeCo/Pt stacking: except for x below 22.2%, all samples have PMA [Fig. 1(a), light green circle]. Replacing Pt with Ir either at the lower interface [Fig. 1(a), purple circle] or at the upper interface [Fig. 1(a), green circle] induces enough PMA to maintain out-of-plane magnetization.

Furthermore, we observe that the interfaces not only play a role on the effective anisotropy but also on the composition for which the magnetic compensation occurs. In this study, the shift of composition of compensation goes up to 6%. Considering the compensation composition with the lowest concentration of Gd (Ta/GdFeCo/Ta), we first notice the need to add more Gd to obtain compensation when Cu is added on top of a Ta buffer. The same behavior is observed for Cu on top of the ferrimagnet. Second, the maximum shift occurs with a copper seed layer and when GdFeCo is directly in contact with Ir and/or Pt.

In the following, we will see why Cu plays a major role in multilayer stacks to obtain PMA and why the composition of the magnetic compensation is modified by the materials in contact with GdFeCo. Because the exchange interaction between conduction electrons is large in Pt, it can exhibit giant magnetic moment induced by magnetic impurities.[9] The proximity of ferromagnetic layers is known to induce indirect ferromagnetic order due to long range oscillatory magnetic exchange interaction called as the Ruderman–Kittel–Kasuya–Yosida (RKKY) interaction. This induces magnetization in Pt either through the Co/Pt interfaces or through the Fe/Pt interfaces.[10–14] At the Fe/Pt interface, the induced magnetic moment on the Pt atoms has been estimated to 0.3 μB,[15] and at the Co/Pt interface, 0.14 μB per Pt atoms have been reported.[16,17] The same applies for TM/Ir interfaces where moment is also induced. The polarization of the Ir interface atoms is estimated at 0.3 μB with Co[18] and 0.2 μB with Fe.[19] Finally, the polarization of the d-band of the Cu atoms is also observed either in Co/Cu multilayers of 0.05 μB[20,21] or in Fe/Cu multilayers up to 0.09 μB.[21] The induced moments in FeCu alloys and in CoCu alloys are similar and around 0.13 μB.[20–22]

Considering that the TM composition of the studied ferrimagnet is roughly 90% of Fe and 10% of Co, we can estimate the polarization of Cu, Ir, and Pt by the FeCo sub-lattice from the literature. The estimations are reported in Fig. 1(b), blue color circle. The evolution of the compensation composition follows the evolution of the magnetic induced moment. Indeed, when Pt or Ir is directly on top of the GdFeCo grown on a Cu layer, the induced moments are maximum among our studied stacks; consequently, additional moment parallel to the FeCo moment has to be taken into account. It is then necessary to add more Gd ($x \approx 29\%$) compared to the other stacks to reach the magnetic compensation point. For Ta/Ir/GdFeCo/Cu/Pt, the compensation is at $x \approx 26.6\%$. This can be explained by a lower intermixing inducing a lower moment at the Ir/GdFeCo interface than at the GdFeCo/Ir interface (see EELS spectra of both multilayers presented in Fig. 3). Since the induced polarization in Cu is much lower, the amount of Gd to be added is also much lower. Finally, for Ta interfaces, no induced polarization was reported, which explains why less Gd is needed ($x \approx 23.9\%$) to achieve compensation. On the contrary, a CoFeB dead layer has been reported in the literature in Ta/CoFeB bilayers.[24] Considering that Gd is not magnetic at room temperature and gets magnetic in contact with the CoFe subnetwork, the compensation composition will not be dependent on this interfacial ferrimagnetic dead layer.

The next step is to elucidate the origin of the magnetic anisotropy in amorphous GdFeCo ferrimagnetics and to explain why, for the same chemical composition, some multilayers show in-plane magnetization and others out-of-plane.

Obviously, as we have seen in the previous paragraph, the magnetic polarization of the interfaces implies an increase in the saturation magnetization and, therefore, the demagnetization field. This explains why among two samples both having a Cu interface, Ta/Cu/

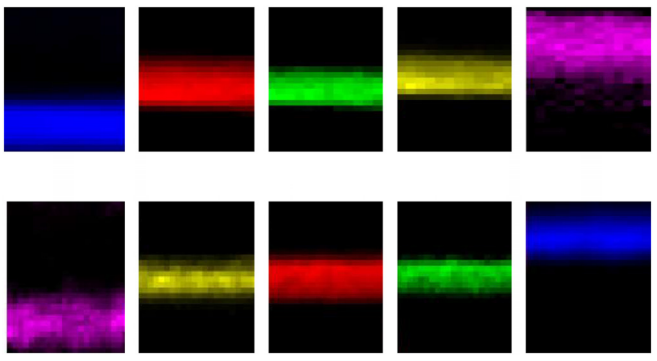

FIG. 3. STEM-EELS elemental maps on Cu/GdFeCo/Ir multilayer (top) and on Ir/GdFeCo/Cu multilayer. Purple: Ir; yellow: Gd; red: Fe; green: Co; blue: Cu.

$Gd_{22.2}FeCo$/Pt is magnetized in-plane while Ta/$Gd_{22.2}FeCo$/Cu/Pt is magnetized out of plane. However, within this framework, we cannot explain other major changes, especially in the case of Ta at each interface where the PMA is particularly small. In the Ta/CoFeB/MgO system, the anisotropy was then correlated with the CoFeB dead layer at the Ta interface. We again must assume that the interfaces play a major role in the anisotropy.

It is well known that after a few nanometers, copper as well as iridium acquire a (111) texture when deposited over an amorphous Ta layer.[23] It is also known that the copper texture has an impact on the perpendicular anisotropy in Fe and Co thin layers.[25,26] This led us to study the magnetic properties as a function of the Cu thickness. Hysteresis loops of Ta(5 nm)/Cu(y nm)/$Gd_{23.4}FeCo$(5 nm)/Pt(5 nm) with y varying from 1 nm to 4 nm are reported in Fig. 4. As can be seen, the Cu thickness has a direct impact on the PMA. For 1 nm of Cu between the Ta and the GdFeCo layers, the magnetization lies clearly in the sample plane with a saturation field around 3200 Oe. For 2 nm, the magnetization remains in-plane but the saturation field is now reduced to about 2400 Oe. At 3 nm Cu, the cycle shows a slight opening, and the saturation field drops to 1200 Oe. At 4 nm, the magnetization is perpendicular to the plane. The field-dependent magnetization cycle is well open. Its shape is typical of the appearance of magnetic domains such as bubbles or skyrmions at a low field. As presented previously, for 5 nm of Cu, the magnetization is perpendicular to the plane at all fields. So, while Cu certainly acquires a strong (111) texture when the thickness increases, the perpendicular saturation field decreases and PMA increases. Nevertheless, at this level, the impact on the crystalline properties GdFeCo (reported as amorphous) was still unknown. Therefore, a local analysis was required to further investigate the details of the local crystallographic structure.

Transmission electron microscopy (TEM) was carried out (Fig. 5). Samples were prepared by focused ion beam (FIB) to mill a cross section. We first observed a Sub/Ta/Cu/$Gd_{24.3}FeCo$/Ir/Pt sample

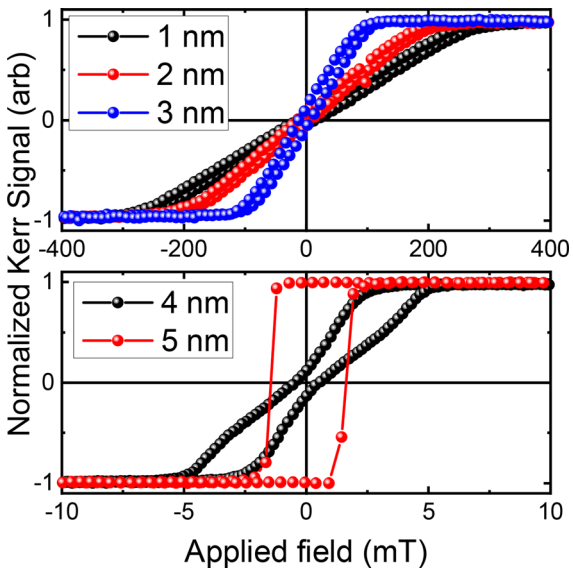

FIG. 4. Kerr hysteresis loops for Ta(5 nm)/Cu(y nm)/$Gd_{23.4}FeCo$(5 nm)/Pt(5 nm) with 1 nm <= y <= 5 nm.

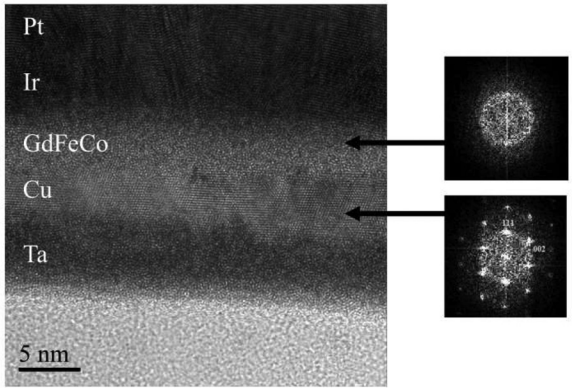

FIG. 5. HRTEM micrograph of Ta/Cu/$Gd_{24.3}FeCo$/Ir/Pt with the FFT of the GdFeCo and Cu layers.

with high-resolution transmission electron microscopy (HRTEM) presented in Fig. 5. The amorphous characteristic of both Ta and GdFeCo layers is confirmed. The Fourier transform (FFT) of the GdFeCo layer shows a diffuse ring pattern characteristic of an amorphous structure. The Cu layer appears as being textured with a growth direction along [111]. The chemical intermixing and roughness seem to be weak at the Cu/GdFeCo interface. We also investigated the reverse order stack Sub/Ta/Ir/$Gd_{24.3}FeCo$/Cu/Pt (not shown). GdFeCo is also clearly amorphous as shown by the FFT that displays again a diffuse ring. As a result, in both samples, no induced texture could be observed in GdFeCo. On the other hand, the Cu layer, either under or on top of GdFeCo, is (111) textured, and the interface with GdFeCo is straight without inter-mixing. In comparison to the other materials studied, Ir also acquires a (111) texture but the interfaces are more intermixed and Ta is fully amorphous. Since there is no visible change in the GdFeCo layer, texture and interface mixing appear to be the key ingredients of PMA. From the TEM images, it was, however, not possible to highlight any texture that could be induced at the GdFeCo interfaces and gradually lost away from the interfaces, but such texture could explain the origin of interfacial anisotropy.

In conclusion, in thin our ultra-thin amorphous rare-earth transition-metal alloys $Gd_x(Fe_{90}Co_{10})_{1-x}$, both compensation composition and anisotropy are found to be strongly depend on the interfaces. While $Gd_x(Fe_{90}Co_{10})_{1-x}$ appears to be amorphous in all combinations of materials and independently on x, (111) textured Cu layers emerge as the best material to promote PMA. In addition, we have shown that the composition for room temperature compensation depends on the magnetic polarizability of the materials at the interface.

This work was supported partly by the French PIA Project "Lorraine Université d'Excellence," Reference No. ANR-15-IDEX-04-LUE, by the "FEDER-FSE Lorraine et Massif Vosges 2014–2020," a European Union Program, and by the Grand Est Region and ICEEL.

AUTHOR DECLARATIONS

Conflict of Interest

The authors have no conflicts to disclose.

Author Contributions

Jean-Loïs Bello: Formal analysis (equal); Investigation (equal); Methodology (equal); Validation (equal). **Daniel Lacour:** Formal analysis (equal); Investigation (equal); Writing – review & editing (equal). **Sylvie Migot:** Formal analysis (equal); Investigation (equal). **Jaafar Ghanbaja:** Formal analysis (equal); Investigation (equal). **Stéphane Mangin:** Funding acquisition (equal); Project administration (equal); Supervision (equal). **Michel Hehn:** Conceptualization (equal); Formal analysis (equal); Investigation (equal); Methodology (equal); Supervision (equal); Validation (equal); Writing – original draft (equal).

DATA AVAILABILITY

The data that support the findings of this study are available from the corresponding author upon reasonable request.

REFERENCES

[1]P. Hansen, S. Klahn, C. Clausen, G. Much, and K. Witter, J. Appl. Phys. **69**, 3194 (1991).
[2]P. Hansen, C. Clausen, G. Much, M. Rosenkranz, and K. Witter, J. Appl. Phys. **66**, 756 (1989).
[3]B. Dieny, I. L. Prejbeanu, K. Garello, P. Gambardella, P. Freitas, R. Lehndorff, W. Raberg, U. Ebels, S. O. Demokritov, J. Akerman *et al.*, Nat. Electron. **3**, 446 (2020).
[4]Y. Xu, M. Deb, G. Malinowski, M. Hehn, W. Zhao, and S. Mangin, Adv. Mater. **29**, 1703474 (2017).
[5]A. Pogorily, E. Shypil, and C. Alexander, J. Magn. Magn. Mater. **286**, 493 (2005).
[6]P. Hansen, J. Magn. Magn. Mater. **83**, 6 (1990).
[7]J. Wei, B. Zhang, M. Hehn, W. Zhang, G. Malinowski, Y. Xu, W. Zhao, and S. Mangin, Phys. Rev. Appl. **15**, 054065 (2021).
[8]D. Cespedes-Berrocal, H. Damas, S. Petit-Watelot, D. Maccariello, P. Tang, A. Arriola-Cordova, P. Vallobra, Y. Xu, J. L. Bello, E. Martin, S. Migot, J. Ghanbaja, S. Zhang, M. Hehn, S. Mangin, C. Panagopoulos, V. Cros, A. Fert, and J. C. Rojas-Sanchez, Adv. Mater. **33**, 2007047 (2021).
[9]A. I. Larkin and V. I. Melnikov, Sov. Phys. JETP. **34**, 656 (1972).
[10]S. S. Parkin, Phys. Rev. Lett. **67**, 3598 (1991).
[11]K. Le Dang, P. Veillet, C. Chappert, R. Farrow, R. Marks, D. Weller, and A. Cebollada, Phys. Rev. B. **50**, 200 (1994).
[12]A. Simopoulos, E. Devlin, A. Kostikas, A. Jankowski, M. Croft, and T. Tsakalakos, Phys. Rev. B. **54**, 9931 (1996).
[13]J. Knepper and F. Yang, Phys. Rev. B. **71**, 224403 (2005).
[14]F. Meier, S. Lounis, J. Wiebe, L. Zhou, S. Heers, P. Mavropoulos, P. H. Dederichs, S. Blügel, and R. Wiesendanger, Phys. Rev. B. **83**, 075407 (2011).
[15]R. Wu, L. Chen, and N. Kioussis, J. Appl. Phys. **79**, 4783 (1996).
[16]T. McGuire, J. Aboaf, and E. Klokholm, J. Appl. Phys. **55**, 1951 (1984).
[17]A. Mukhopadhyay, S. K. Vayalil, D. Graulich, I. Ahamed, S. Francoual, A. Kashyap, T. Kuschel, and P. A. Kumar, Phys. Rev. B. **102**, 144435 (2020).
[18]M. Perini, S. Meyer, B. Dupé, S. V. Malottki, A. Kubetzka, K. V. Bergmann, R. Wiesendanger, and S. Heinze, Phys. Rev. B. **97**, 184425 (2018).
[19]F. Wilhelm, P. Poulopoulos, H. Wende, A. Scherz, K. Baberschke, M. Angelakeris, N. Flevaris, and A. Rogalev, Phys. Rev. Lett. **87**, 207202 (2001).
[20]M. Samant, J. Stöhr, S. Parkin, G. Held, B. Hermsmeier, F. Herman, M. van Schilfgaarde, L.-C. Duda, D. Mancini, N. Wassdahl *et al.*, Phys. Rev. Lett. **72**, 1112 (1994).
[21]G. Held, M. Samant, J. Stöhr, B. Hermsmeier, M. Schilfgaarde, and R. Nakajimas, Z. Phys. B Condens. Matter. **100**, 335 (1997).
[22]W. Kuch, M. Salvietti, X. Gao, M. Klaua, J. Barthel, C. V. Mohan, and J. Kirschner, J. Appl. Phys. **83**, 7019 (1998).
[23]I. L. Castro, V. P. Nascimento, E. C. Passamani, A. Y. Takeuchi, C. Larica, M. Tafur, and F. Pelegrini, J. Appl. Phys. **113**, 203903 (2013).
[24]S. Shen, D.-S. Lee, C.-W. Cheng, W.-J. Chan, and G. Chern, IEEE Trans. Mag. **55**, 1 (2019).
[25]F. Huang, G. J. Mankey, and R. F. Willis, J. Appl. Phys. **75**, 6406 (1994).
[26]M. T. Kief and W. F. Egelhoff, J. Appl. Phys. **73**, 6195 (1993).